Real-Time 3D Electrical Impedance Imaging for Ventilation Monitoring of the Lung: Pilot study

Bruce Amm, *Member, IEEE*, Tzu-Jen Kao, Xin Wang, Gregory Boverman, *Member, IEEE*, David Shoudy, James Sabatini, Jeffrey Ashe, Jonathan Newell, *Senior Member, IEEE*, Gary Saulnier, *Senior Member, IEEE,* David Isaacson, *Senior Member, IEEE*, David Davenport

***Abstract*— We report an Electrical Impedance Tomography device capable of detecting gravity-induced regional ventilation changes in real-time without averaging or using a contrast medium. Changes in lung ventilation are demonstrated in right and left lateral decubitus position and compared to those seen in an upright and supine normal subject.**

I. Introduction

Electrical Impedance Imaging, also called Electrical Impedance Tomography (EIT), is a non-invasive, radiation-free imaging technique taking advantage of differences in electrical properties of biological material. Different materials, such as fat, muscle, blood, and air show different electrical properties (resistivity or conductance). The electrical properties of the material also depend on the condition of the tissue such as its air content (ventilation), blood-content (perfusion), or water-content (hydration). Images of the electrical property thus reflect the condition of the tissue or organ.

The first practical medical application of EIT was demonstrated by Brown *et al.* [1,2], who developed the first EIT system (Sheffield Mark I) for research purposes in the mid-80's. Since then, proposed areas of medical application has been expanded to breast, skin, brain, lung, heart, limbs, and the gastrointestinal tract [3]. While the breakthrough to routine clinical use is still pending, initial commercial offerings are beginning to appear, such as the Drager PulmoVista 500, for observing the regional effects of mechanical ventilation [4].

The PulmoVista 500 uses 16 metal ECG electrodes placed around the chest at the sixth intercostal space and EIT data are generated by applying alternating current (50 kHz, 5 mA peak-to-peak) to pairs of electrodes in a sequential rotating process and measuring the resulting voltage differences between neighboring electrodes. Two-dimensional impedance images were subsequently generated from a reconstruction algorithm based on a finite element model [5].

The 2D reconstruction algorithm is used for 2D electrode configurations on 3D test phantoms or the thorax of human subject. Therefore, the impedance distribution shown on the 2D plane of the reconstructed images does not exactly represent the electrical properties of the cross section, since some of the EIT currents flow above and below the plane of the electrodes. Thus, using a 2D plane to represent a 3D thorax may cause a misinterpretation of the condition of the lungs.

To better present the ventilation status of the lung, Goble *et al.* [6] in 1990 reported the development of a 3D reconstruction algorithm using an electrode array having 16 electrodes in each of four layers around a cylindrical geometry. Metherall *et al.* also reported in 1996 [7] a 3D algorithm using four layers of 16 electrodes and studies of the thorax of healthy human subjects.

The main focus of this paper is to present, using our prototype EIT system, a 3D reconstruction algorithm and demonstrate its use to show ventilation differences in a volunteer human subject in various postures.

II. Method

A. EIT System - GENESIS

Our prototype EIT system (Fig. 1), called the General Electric Non-invasive Electrical impedance Spectroscopy Imaging System (GENESIS), is a parallel drive instrument, similar to the RPI ACT3 architecture [10], employing

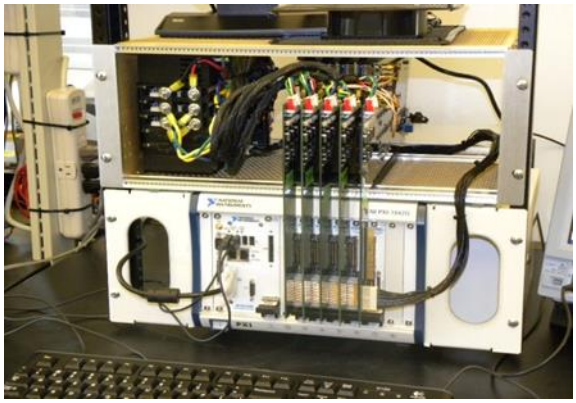

Figure 1. GENESIS: Prototype EIT system

Research supported by Grant Number 1R01HL109854-01 from the National Heart, Lung and Blood Institute. The content is solely the responsibility of the authors and does not necessarily represent the official views of the National Institutes of Health

B Amm, T Kao, D Shoudy, J Sabatini, X Wang, G Boverman, J Ashe, and D Davenport are with GE Global Research Center, Niskayuna NY 12309 USA.

J. Newell, G Saulnier, and D Isaacson are with the Rensselaer Polytechnic Institute, Troy, NY 12180 USA

modified-Howland current sources compensated with Negative Impedance Converters (NIC). Each compensated current source is paired with voltage measurement circuitry for simultaneous current drive and voltage measurement through each electrode. The parallel drive architecture supports driving up to 32 independent current sources and measuring 32 independent voltage channels simultaneously.

Each current source is tuned for high output impedance by adjusting the Howland and NIC circuits, under program control, to an operating point where the combined Howland output resistance, output capacitance, and remaining parasitic capacitances are cancelled by a negative resistance and negative capacitance from the NIC to produce a net high output impedance. Impedance is measured using the droop circuit method [10], and stability of this circuit architecture is obtained by careful compensation of the modified-Howland and NIC.

Coherent modulation and demodulation of a 10 kHz carrier is implemented using field programmable gate arrays, and frame rates in excess of 20 per second are supported by the system, where each frame contains up to 64 current patterns. One-step reconstruction is performed, and the result displayed in real-time for each frame, and raw data is stored for further offline analysis.

B. 3D Reconstruction Algorithm

We employed a linear reconstruction algorithm adopted from the Rensselaer TodLeR algorithm [8,9] to extract the impedance changes due to the ventilation status of the lung. A brief summary of the reconstruction is as follows:

1. At two time instants t_0 and t, apply designed current patterns I_l^k and measure the corresponding voltages V_l^k on electrodes labeled with the subscript $l = 1, \ldots L$ for $K = 1, \ldots L-1$. Use the notation $\delta\sigma = \sigma - \sigma_0$ and the approximation $U = U_0 + 0(\delta\sigma)$, where U denotes the measured voltage at t_0 and U_0 is the voltage that would have been measured if the conductivity were uniform (σ_0) in the volume, to obtain the equations relating measured current voltages to moments of the unknown conductivity,

$$D(k,x) = \sum_{l=1}^{L} V_l^k(\sigma_0) I_l^x - V_l^x(\sigma) I_l^k = \int_B \delta\sigma \nabla U_0^k \cdot \nabla U_0^x dp + O(\delta\sigma^2)$$

where $D(k,x)$ is the "data" matrix used to reconstruct the change in conductivity between the two time points.

2. Choose a basis function $\{\Phi_n(p)\}_{n=1}^N$ where N is the number of voxels in the predefined reconstruction mesh for the approximation $\delta\sigma(p) = \sum_{n=1}^N \delta\sigma_n \Phi_n(p)$ and compute a coefficient matrix A,

$$A_{k,x,n} = \int_{Vn} \Phi_n(p) \nabla U_0^k \cdot \nabla U_0^x dp$$

where V_n is the spatial extent of voxel n.

3. Solve the equation $\delta\sigma = \left(A^T A + \varepsilon R\right)^{-1} \times A^T D$ and display $\delta\sigma$ on the predefined mesh, 496-Joshua tree mesh [12] for each layer. Here, R denotes the regularization matrix and ε denotes the regularization parameter.

Further detail on the current pattern design and reconstruction algorithm can be found in [12].

The global impedance changes were calculated to fit the best constant approximation to the reference point of measured voltages. It can be computed from the following formula.

$$\rho = \sum_{k=1}^{K}\sum_{l=1}^{L} U_l^k V_l^k \Big/ \sum_{k=1}^{K}\sum_{l=1}^{L} U_l^k U_l^k$$

Again, U and V denote the measured voltages at t_0 and t respectively. The detailed derivation has been mentioned by Mueller *et al.* [11].

C. Reconstruction verification

To verify the reconstruction algorithm, it was first tested on the saline test tank shown in Fig. 2. The cylindrical tank is 27.5 cm high and 30 cm in diameter. Stainless steel electrodes 3 cm in diameter are arrayed in two rings around the tank with a center-to-center distance of 5.5 cm between the rings. The tank was filled with tap water and a plastic ball 1.5 inch in diameter was suspended at the bottom layer of the electrode plane. The conductivity of the water was approximately 45 mS/m.

D. Human subject study

Thirty-two ECG-type electrodes were placed around the chest of a healthy human subject in 2 circular rings. The top ring was placed at the fourth intercostal space and the bottom at the sixth intercostal space. A reference ground electrode was placed on the shoulder. The electrode size was 3 cm in diameter.

To better correlate to the breathing cycle, the subject breathed through a Biopac system spirometer. The subject was studied first upright, then supine, then left-lateral

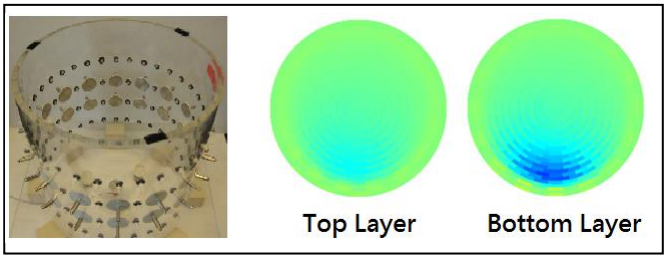

Figure 2. Left: the saline test tank, Middle and Right: reconstructed images, where blue indicates an area of reduced conductivity

decubitus, then right lateral decubitus, and finally again upright. The subject performed a series of respiratory maneuvers in each posture: normal breathing (60s), deep breathing (60s), breath holding (30s), and then normal breathing again (30s).

The reconstruction algorithm was embedded in our prototype GENESIS system. With the present hardware setup, the system generated reconstructed images at 19 frames per second to monitor the subject in real-time.

III. Results

Fig. 3 shows the respiration data of a volunteer human subject with a BMI of 23.5. The EIT global impedance (red) has also been plotted and matches well with the spirometer (blue) curve during all ventilatory maneuvers. To plot spirometer and global impedance changes in one figure, we normalized both waveforms to make the envelope of each waveform have amplitude 1.

The reconstructed images (Fig. 4) show volume changes at end inspiration (approx. frame 40) using the start of inspiration (frame 0) as the reference. Blue regions indicate reduced conductivity while red regions are increased conductivity. The near plane of the rendering is anterior and the top plane is superior (as if the subject were facing the viewer). From left to right the images represent upright, supine, left lateral and right lateral decubitus positions. The lower panels show maximum (single voxel) and average conductivity changes vs. time in the left lung and right lung region, again using the start of inspiration as the reference. The average change was calculated by averaging over the left and right dorsal quadrants in the upper ring. The maximum change with inspiration in the supine posture was about -300 units in both lungs. With deep breathing, this increased to about -700 units, with corresponding increases seen under all other postures (Fig. 5). The images and traces

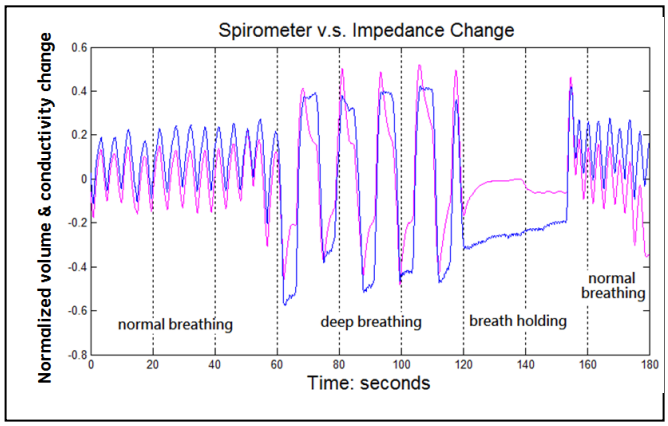

Figure 3. Normalized Spirometer (blue) vs Global Impedance Change (red)

in Figs. 4 and 5 were constructed in real-time at nearly 20 frames/sec, without averaging and without contrast agents. The conductivity changes for the given postures are summarized in Fig. 6.

IV. Discussion

The key findings of both Fig. 4 and Fig. 5, that correlate well with the physiological effects, is that the dependent (gravitationally lower) lung has an greater ventilation than the higher lung. While in upright and supine posture, the conductivity changes in both lungs are nearly comparable, with left lung dependent, the left lung trace (blue/green) change is significantly larger. With the right lung dependent, its change (red/purple) becomes appreciably larger than that of the left. As summarized in Fig. 6, this result of greater ventilation in the dependent lung is as expected in spontaneous breathing [13]. This is due to the gravity gradient and to the fact that the lower diaphragm is able to contract more efficiently during spontaneous respiration

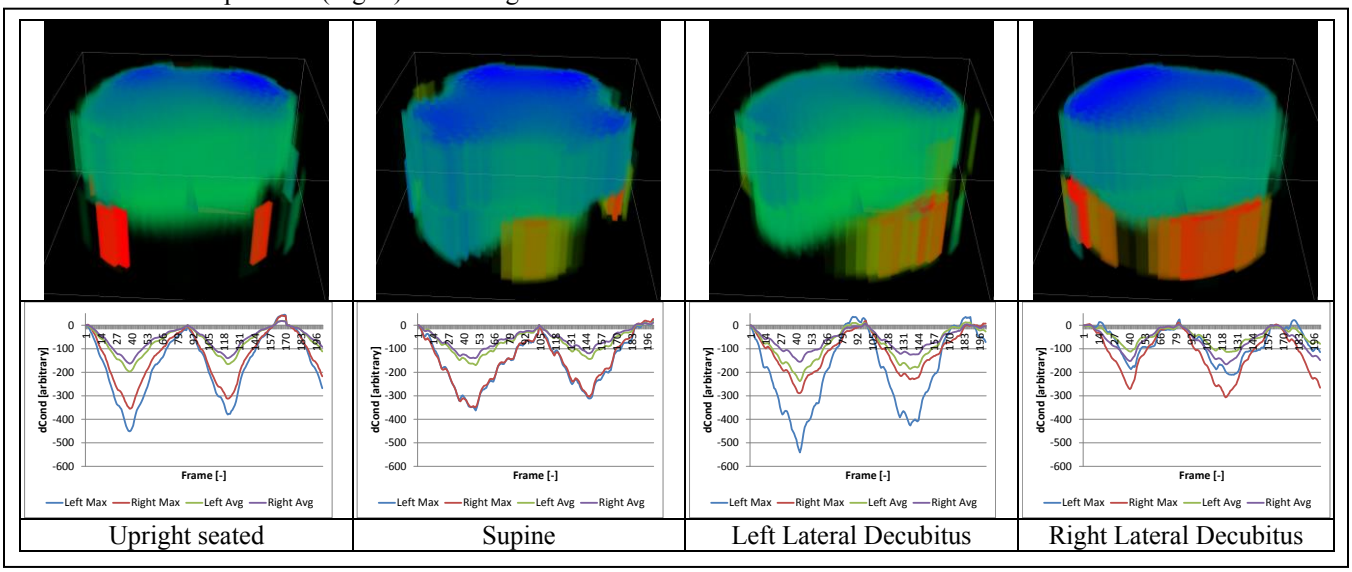

Figure 4. Normal breathing from left to right: upright seated, supine, left lateral, and right lateral. Top: image of end inhalation using begin inhalation as a reference, blue indicates regions of lower conductivity, near plane of the image is anterior, top plane is superior (as if the subject were facing the viewer). Bottom : 200 frame (~10 seconds) conductivity time traces (aribtrary units), of the maximum and average conductivity change in the left lung and right lung region

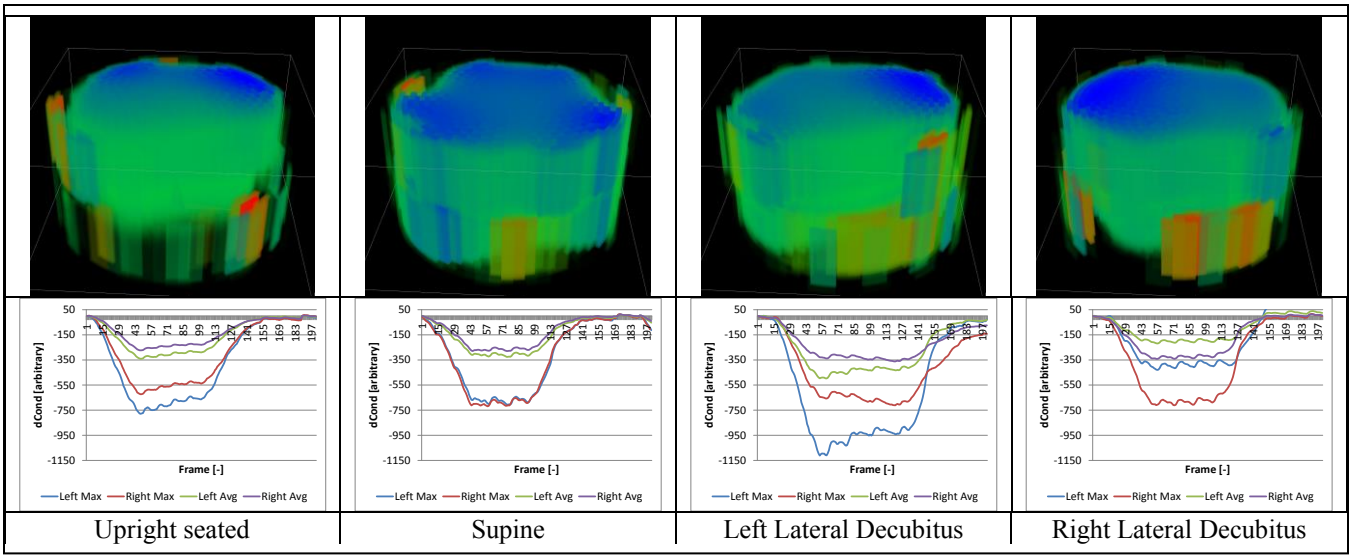

Figure 5. Deep breathing images and conductivity traces, images and panel order as described in Fig. 4

causing the dependent lung to fill more [14].

V. Conclusion

We have demonstrated our EIT device's ability to detect in three dimensions and real time, the gravity-induced changes in ventilation during both normal and deep breathing without averaging or contrast media.

VI. References

[1] D. C. Barber and B. H. Brown, "Applied potential tomography," *Journal of Physics E: Scientific Instruments,* vol. 17, no. 9, pp. 723-733, 1984.

[2] B. H. Brown, D. C. Barber and A. D. Seagar, "Applied potential tomography: possible clinical applications," *Clinical Physics and Physiological Measurement,* vol. 6, no. 2, pp. 109-121, 1985.

[3] D. S. Holder, Ed., Electrical Impedance Tomography: Methods, History and Applications, Taylor and Francis, 2004.

[4] [Online]. Available: http://campaigns.draeger.com/pulmovista500/en/. [Accessed March 2014].

[5] C. Putensen, H. Wrigge and J. Zinserling, "Electrical impedance tomography guided ventilation therapy," *Curr Opin Crit Care,* vol. 13, no. 3, pp. 344-50, 2007.

[6] J. Goble and D. Isaacson, "Fast reconstruction algorithms for three-dimensional electrical impedance tomography," in *Engineering in Medicine and Biology Society, 1990, Proceedings of the Twelfth Annual International Conference of the IEEE*, 1990.

[7] D. C. Metherall, D. C. Barber, R. H. Smallwood and B. H. Brown, "Three-dimensional electrical impedance tomography," *Nature,* vol. 380, pp. 509-512, 1996.

[8] R. S. Blue, D. Isaacson and N. J. C, "Real-time three-dimensional electrical impedance imaging," *Physiol Meas,* vol. 21, no. 1, pp. 15-26, 2000.

[9] R. S. Blue, *Real-Time Three-Dimensional Electrical Impedance Tomography,* Troy, NY: Rensselar Polytechnic Institute, 1997.

[10] R. D. Cook, G. J. Saulnier, D. G. Gisser, J. C. Goble, J. C. Newell and D. Isaacson, "ACT3: A High-speed, High-Precision Electrical Impedance Tomograph," *IEEE Trans on Biomed Eng,* vol. 41, no. 8, pp. 713-722, 1994.

[11] J. L. Mueller, D. Isaacson and N. J. C, "A reconstruction algorithm for electrical impedance tomography data collected on rectangular electrode arrays," *IEEE Trans Biomed Eng,* vol. 46, no. 11, pp. 1379-1386, 1999.

[12] T.-J. Kao, B. S. Kim, D. Isaaxson, J. C. Newell and G. J. Saulnier, "Reducing boundary effects in static EIT imaging," *Physiol Meas,* vol. 27, no. 5, pp. S81-S91, 2006.

[13] K. Kaneko, J. Milic-Emili, M. B. Dolovich, A. Dawson and D. V. Bates, "Regional distribution of ventilation and perfusion as a function of body position," *Journal of Applied Physiology,* vol. 21, no. 3, pp. 767-777, May 1966.

[14] M. J. Tobin, Ed., "Principles And Practice of Mechanical Ventilation," in *Principles And Practice of Mechanical Ventilation*, 3rd ed., McGraw-Hill Professional, 2012, p. 306.

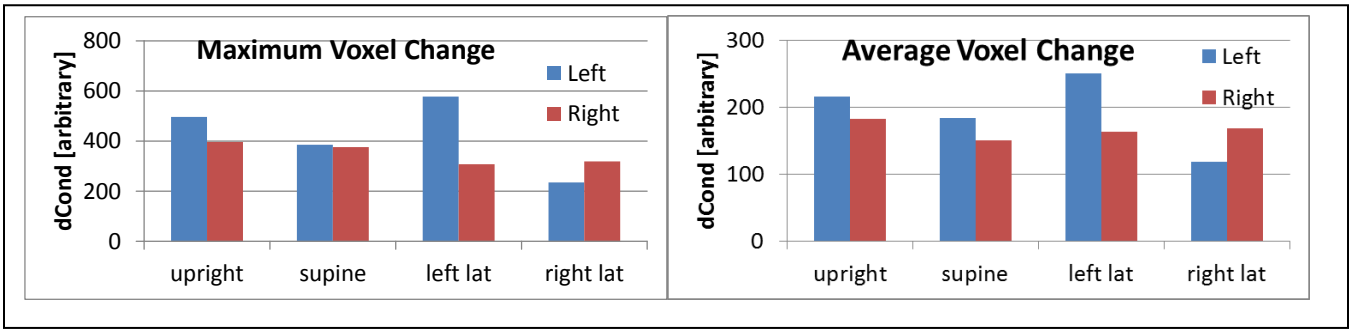

Figure 6. Maximum and average conductivity changes (dCond) in the right and left lung region for the specified postures